Application of digital interferogram evaluation techniques to the measurement of 3-D flow fields

Friedhelm Becker and Yung H. Yu

Aeromechanics Laboratory (AVSCOM)

NASA Ames Research Center

Moffett Field, California 94035, USA

Contents

Abstract

A system for digital interferogram evaluation has been implemented based on an image processing system connected to a host computer. The system supports one and two-dimensional interferogram evaluations. Interferograms are digitized, enhanced and segmented. The fringe coordinates are extracted and the fringes are represented as polygon data structures. Fringe numbering and fringe interpolation modules are implemented. The system supports editing and interactive features as well as graphic visualization. An application of the system to the evaluation of double exposure interferograms from the transonic flow field around a helicopter blade and the reconstruction of the 3-D flow field is given.

Keywords: automatic fringe analysis, interferometry, digital image processing, transonic flows, holographic techniques

1. Introduction

Holographic interferometric techniques have been widely used in recent years in the area of aerodynamics for flow visualization and quantitative measurement of flow properties, particularly for large field measurements in two- and three-dimensional transonic flows [1-4].

Interferometric techniques measure the optical pathlength differences (OPD) between the actual refractive index field $n(x,y,z)$ and a reference field n_o, in either the undisturbed flow or the test section without flow. The path length differences in the plane of observation, measured along the probing rays L in units of the wavelength λ, are registered as phase shifts $\Delta\psi$ of the fringes in an interferogram

$$OPD = \frac{\Delta\psi\lambda}{2\pi} = \int_L [n - n_o]\, ds = N\lambda \qquad (1)$$

where N is the fringe order number. The fringes in an interferogram represent contour lines of equal OPD.

In the two-dimensional case where a constant refractive index along the probing rays is assumed, the OPD is directly related to the refractive index and one interferogram is sufficient to obtain the flow field at any interesting location in the field of view.

In the general case, however, where the flow field is asymmetric, a set of interferograms has to be recorded at different viewing angles around the field to reconstruct the flow field. Such an interferogram is a projection of the index of the refractive index field as it represents line integrals of a scalar variable along rays. In general the line integral can be written:

$$N_\phi(\xi,z) = \frac{1}{\lambda} \int_{L_\phi(\xi,z)} [n(x,y,z) - n_o]\, ds \qquad (2)$$

where (ξ,z) denote the coordinates in the interferogram plane and $L_\phi(\xi,z)$ is a pathlength through the object.

The refractive index at any given point in the flow field may be obtained by applying computer assisted tomography (CAT) methods to invert the integral equation (2). In the refractionless limit, which is assumed here, the light rays passing through a horizontal plane (z=const) of the phase object form the fringe order function along a straight horizontal line in the interferogram plane. This assumption which is valid in the actual application, as shown by a numerical simulation [5], considerably simplifies the numerical reconstuction procedure, because it allows to reduce the 3-D reconstruction problem to a 2-D one by processing horizontal planes independently.

One important step between recording interferograms and applying tomographic reconstruction techniques, however, is the evaluation of

interferograms: reading fringe positions and fringe numbers. Up to now, most interferograms from aerodynamic tests have to be evaluated by either reading fringe numbers and its positions manually or by tracing the fringe lines by hand with the help of a tracking device (for instance a graphic tablet). Manual evaluation, however, is a very time consuming and inaccurate procedure. It is evident that in the current application, where large numbers of interferograms have to be evaluated at several horizontal planes, utilization of an automatic fringe reading procedure would enhance the evaluation considerably and would make the interferometric technique a much more powerful measurement tool.

There are some different approaches to automatize the interferogram analysis. One is direct phase measurement interferometry which uses phase shifting or heterodyne techniques to obtain a set of phase-shifted interferograms from which a relative phase at any given point in the plane of observation may be calculated [6-10]. A similar approach is point by point electronic phase measurement using heterodyne interferometry [11]. Both methods have been used for measuring deformations of opaque solid objects in nondestructive testing and for surface measurements in optical quality testing. Phase measurements on a point by point basis may be very precise, but are inherently slow and need a high acquisition time. The application of phase shifting techniques requires real time test environments, simultaneous recording of multiple phase shifted images, or multiple reference beam holography.

By introducing enough tilt into the interferometric system (finite fringe interferometry) it is possible to restrict the fringe field to a straight line type pattern. This may then be evaluated by using Fourier techniques [12], or spatial synchronous phase detection [13]. These techniques require high fringe densities and therefore a high resolution detection. Processing times are also very high.

Other approaches involve the use of image processing systems to enable a computer aided evaluation of the real fringe pattern. This systems usually digitize and digitally enhance the fringe pattern. Some perform one dimensional fringe analysis for nondestructive testing applications [14-16], locate fringe centers [17] or fringe sides [18-22] or trace the fringe extrema [23] in two dimenional analysis implementations. Interactive, computer-based systems allow the implementation of sophisticated algorithms for image enhancement, fringe segmentation, error correction and fringe numbering, which have to be applied for the evaluation of conventionally observed interferograms. Often the introduction of sufficient tilt (as e.g. in [19]) into the interferometric systems used in fluid mechanics is not feasible, so the fringe patterns are generally of higher complexity.

In this paper, digital interferogram analysis methods developed previously by one of the authors [20,21], implemented on an image processing system, will be described in more details and will be applied to the reconstruction of 3-D transonic flow fields around a rotor blade.

2. Experimental setup and holographic recording

The double exposure holographic interferograms of the flow near a hovering 1/7 geometrically scaled model UH-1H rotor were recently recorded. The one blade rotor system, 1.05 m of the span and 0.075 m chord length with NACA 0012 airfoil sections, was run at a tip Mach number of 0.9 in the anechoic hover chamber at Aeromechanics Lab. A pulsed ruby laser was used to record the double exposed holograms of the transonic flow field around the blade. The diameter of the object beam was 0.6 m, and the total path length was about 30 m.

The first exposure was recorded with the rotor stationary while the second exposure was recorded with the blade rotating by synchronizing the laser pulse with the desired blade position. A more detailed description of the holographic system and the rotor test is given in [3].

Fig. 1 shows a top view of the set-up with a few typical interferograms recorded at different azimuthal angles. Interferograms at 40 different views were recorded at 2 degree intervals. In Fig. 1, interferograms recorded at angles around 90 degrees have very few or no fringes, because the optical rays pass through a very thin portion of the refractive index field. Interferograms recorded around 180 degrees however contain many fringes as the optical rays pass through the longest portion of the refractive index field along the

blade. In some of these interferograms shock waves are present. Parts of the fringe pattern are blocked off by the shadow of the rotor system in several interferograms.

3. Interferogram evaluation

In order to reconstruct the 3-D flow field from these interferograms, using tomographic reconstruction techniques, the fringe number functions along cross-sections of a plane parallel to the rotor disk are required. Data from all the views are needed to reconstruct the index of refraction in a particular plane above the blade. Several planes have to be reconstructed in order to get a 3-D flow field representation. This procedure requires each interferogram be represented in a form which allows computing the fringe order function at any desired point.

Interferogram evaluation means to extract lines of equal phase $\Delta\psi$ (equal OPD) from the intensity $I(x,y)$ in the two-dimensional interferogram plane which may be written as

$$I(x,y) = I_0(x,y) + I_1(x,y)\cos(\Delta\psi). \qquad (3)$$

The term I_0 describes the background illumination and the distortions, and I_1 is a modulation term. Both may vary over the field of view. The fringe's maxima, minima, or the fringe's sides are easily detectable

lines of equal phase. Each fringe has to be recognized (segmented) from its surrounding and those pixels which represent the constant phase line have to be picked up. In the simplest case where the fringe field is a sinusoidal pattern without any distortions (uniform background-illumination), the segmentation can be done by thresholding (level-clipping) using the mean gray value. This procedure would give the fringe-sides as constant phase lines.

Most of the holographic interferograms however have a nonuniform background illumination with varying contrast and several other distortions (speckle noise, electronic noise). The fringe segmentation in this case has to be somewhat more sophisticated to enable a trouble free postprocessing of the extracted data.

Another difficulty in evaluation of interferograms from transonic flows is the large variation in fringe density. In all of the near spanwise views, the fringes are very narrow above the blade, but are very wide in the rest of the field (see Fig. 1). Also the fringe frequency may change rather rapidly across the field, especially if a shock is present. In applying tomographic reconstruction techniques it is important to know the flow field over the entire field of view with high accuracy. This requirement, however, conflicts with the restricted resolution of the image processing system. A resolving power of more than 3000 pixels across the field of view would have been necessary to evaluate these interferograms. In order to achieve the same resolution with the available system blown-up parts of the

interferograms had to be processed individually and had to be merged subsequently.

The interferogram evaluation by computer aided methods can be subdivided into the following steps: digitization of the interferograms and image enhancement, fringe segmentation and fringe coordinate extraction, merging of fringe fields obtainded from several magnified views, fringe numbering and correction of fringe disconnections, coordinate transformations, interpolation and extrapolation of fringe number functions and finally, reconstruction of the flow field, conversion of fringe numbers into refractive index and interesting flow properties.

In the following, an interferogram evaluation system will be described, which supports all of the evaluation steps mentioned above. All the modules may be called interactively or in batch mode. An editing feature is also implemented, which allows supervision of the evaluation, correction of extraction errors, input of information by hand, modification of fringe numbers and excessive graphic visualization.

3.1 Hardware components

An image processing system (De Anza IP-6400) connected to a VAX 11/780 host computer features the main hardware to digitize the interferograms and to do some image enhancement processing as shown in Fig. 2.

The resolution of the system is 512 x 512 pixels with an 8 bit intensity range. Currently it is equipped with two of possible four memory planes as well as a graphic and an alpha numeric overlay.

A frame-grabbing unit is able to digitize a frame of a video-signal in real time (1/30 sec). A black and white video-camera (MTI series 68) with a resolution (bandwidth) of 18 MHz is connected to this input channel.

The system has an arithmetic-logic-unit (ALU), with which a real-time addition, subtraction or comparison of one or more image-planes may be made. The contents of each memory-plane may be routed through look-up-tables before input to the ALU, to the video-output-processor or to another plane. The actual contents of any or a combination of the image planes is output via a video-output-processor and can be shown on a color-display. Each channel has its own color-mapping tables.

A joystick control device is used for interactive input. It controls two cursors, which may be used in a number of different operating modes. A color print system (Dunn Instruments model 631) serves as a hardcopy device for the color monitor.

3.2. Digitization and preprocessing

During the recording of the holographic interferograms, two fiducial points were marked in the image plane with a known position relative to the rotor system. This allows a subsequent coordinate transformation into a space fixed coordinate system.

Each interferogram was then digitized over an area of about 0.18 x 0.25 m^2 with several enlarged subsections, depending on the fringe density in the interferograms. A scale, aligned to the fiducial marks, was always digitized together with the interferogram to be able to identify the position and the magnification of the enlarged segments.

Before segmentation and fringe coordinate extraction are applied it may be useful to do some image enhancement to reduce noise. Frame averaging methods increase the signal-to-noise-ratio of the imaging electronic components, thereby improving the picture quality. The averaging is implemented in real time, over 30 frames in one second. A spatial smoothing in a 3 x 3 kernel or in an N x M kernel is useful to reduce high frequency noise introduced by the holographic procedure like speckle noise. A histogram equalization may also be done to improve the visibility of a fringe pattern on the display. But our experience is that this technique has to be used with care because it is a nonlinear transformation and it tends to amplify noise.

3.3. One dimensional evaluation

A one-dimensional interactive processing may be employed, if only one 2-D plane of the flow field is reconstructed, and hence only one cross section through each interferogram has to be known. In this case some of the overhead required for the full two dimensional evaluation of the fringe pattern may be avoided. But the procedure has to be interactive, because local information (i.e. knowledge of the fringe locations along one line) is not sufficient to number the fringes correctly or to detect lost fringes or other distortions. In an interactive procedure the information such as acceptance of the segmentation and assigning of fringe numbers has to be given by the user.

Several methods have been reported for pattern segmentation which involve gradient operators [24], adaptive thresholding [25], Fourier transforms [15] or piecewise approximation of elementary functions [26,27]. The gradient operators, often used in line detection algorithms, are easy to implement, but don't work well on sinusoidal patterns. They are also very noise sensitive. Adaptive thresholding methods are often used for document scanning and character recognition. They too fail on sinusoidal images. Fourier transform methods are difficult to adapt to fringe fields with varying fringe frequencies across the scan line. Also they require a certain number of fringes in the cross section and are mainly used for detecting phase shifts in patterns of parallel and equidistant fringes. The piecewise approximation of sinusoidal functions or polynomials has been used in a number of cases where precise phase measurements had to be

made in the presence of speckle noise with only a few fringes in the cross section. These methods generally require excessive computing time and the convergence and stability depends on a priori estimates of the fringe positions.

A floating threshold method [20] has been used here for segmentation. This is a two pass scheme. In the first pass the scan line is searched for extrema using a hysteresis detection scheme. A local extremum is only accepted, if it has a minimum gray value difference to the last accepted extremum of different type (after a minimum was accepted, it will be searched for a maximum and vice versa). With the minimum gray value difference, a noise rejection threshold is established. With the found extrema, a steplike threshold function is defined, which settles at the mean gray value between adjacent extrema. Comparison of this function with the original scan line then yields a binary fringe pattern. The transitions from black to white and white to black define the positions of the left and right fringe sides (see Fig. 3a). This method is fast and quite robust and works well even on fringe fields with abrupt changes in image brightness, fringe density, and contrast. The value of the acceptance threshold is not critical and may usually be varied in a wide range without affecting the segmentation. Also the recognized fringe positions do not depend on the actual value of the acceptance threshold. In images with a known modulation variation a spatially dependent acceptance threshold may be used [20].

An example of the segmentation applied to a typical interferogram

is shown in Fig. 3b. The actual intensity of a part of the scan line is plotted as a solid line and the extracted fringe-positions (left and right sides) are shown as dotted lines.

A program featuring the one-dimensional evaluation digitizes and preprocesses an interferogram and does a fringe segmentation along a line or a set of lines through the field of view. The result of the segmentation procedure (a binary fringe pattern) is written back to the image screen for monitoring reasons (see Fig. 3c,d). The user may interactively change the acceptance threshold or edit the segmented cross section in heavily distorted regions before he continues to the numbering section. The cursor can be moved to each part of the segmented line, and fringe numbers may be assigned interactively by various commands. The task of assigning fringe numbers is supported by color coding the black parts of the fringes which shows whether the fringe order function increases or decreses by one, or if a discontinuity is present between adjacent fringes. The resulting fringe order function may also be plotted onto a graphic terminal.

A postprocessing program merges all the data taken from different enlarged portions of an interferogram (as shown in Fig. 3c,d) and uses a spline-approximation to interpolate between the fringes. The left- and right-side coordinates, or the middle of the white or black parts of the fringes may be taken as nodes for the spline approximation. To allow discontinuities in the fringe-order function, a rational spline approximation is used. The type of approximation

here may be changed gradually from 1st order to 3rd order polynomials using a parameter derived from the slope of the OPD-function (see Fig. 3e).

3.4. Two dimensional interactive processing

Often the knowledge of only a cross section across the field of view is not sufficient to interpret a given flow problem, but the fringe patterns have to be evaluated over the whole field of view. To facilitate the two-dimensional interferogram evaluation, additional algorithms have been implemented to segment fringes, to extract each fringe's coordinates (trace the fringe sides), and represent the whole fringe field as a polygon data structure. Methods for numbering these line fields and detecting extraction errors have been developed. With a two-dimensional interpolation scheme fractional fringe order numbers may then be estimated at any given point in the field of view. The methods for two-dimensional evaluation will be discussed in the following paragraphs. Typical execution times of the most frequently used modules are given in Table 1.

3.4.1 Segmentation, polygon representation

The fringe segmentation in the two-dimensional case could be done using the same one-dimensional floating threshold method as described above in a sequential manner for each of the lines of an image. This

generally works well for fringe fields running more or less perpendicular to the scan-line, however it may fail if the fringes have significant components parallel to the scan-line and noise or background modulations are present. An example is shown in Fig. 4, where the floating threshold method with fixed acceptance treshold has been applied to a digitized fringe field of low quality in Fig. 4a. The resulting binary pattern are shown after the technique was applied to lines (Fig. 4b) or to columns (Fig. 4c).

A truly 2-dimensional technique would be to subtract the nonuniform background and subsequently apply a thresholding with the mean gray value. In the case of dual reference beam holography the background correction could be done by subtracting a 180° phase shifted interferogram [14]. In our case the approximate background has to be derived from the fringe field itself by a process called "very low pass" filtering. This technique was also used in [17], each pixel was replaced by the mean gray value in a relatively large window. To save computing time the image area is divided into meshes of suitable size (e.g. 64 x 64 pixels) and the mean gray values are estimated in these meshes. A surface approximation is then constructed by bilinear interpolation between the gray values in every four adjacent mesh points. The discontinuities at the mesh boundaries due to the bilinear interpolation do not affect the segmentation. This surface is then subtracted from the original interferogram where an offset of 128 is added to all pixels to avoid negative intensities. An example

of the background subtraction is given in Fig. 4d. A thresholding at level 128 was performed after subtracting the approximated background illumination, from the original image in Fig. 4a. The background was constructed on a grid with meshsize 64 x 64. The method works better than the floating thresholding in most parts of the image, but doesn't work as well in the low contrast areas in the lower middle of the interferogram and in the region of the shock. In the interactive mode all the above mentioned methods may be combined so that each one works on the whole picture or in selected areas only. So it is possible to use the best suited method for each part of the image. Fig. 4e shows the resulting binary pattern after combining background subtraction with horizontal and vertical floating thresholding. After binarization, binary smoothing or shrinking-expanding operations can be applied to reduce pepper and salt noise and to fill in broken lines or truncate line artifacts as shown in Fig. 4f.

Coordinate extraction

After applying the segmentation procedures, the fringe field is transformed into a binary tone pattern. In some applications the binary fringe pattern are reduced to a line representation using skeletonization techniques [17-19], giving the middle of the black (or white) fringes as the fringe positions. In our implementation the coordinates of the fringes are determined at the transition from white to black (and vice versa) giving the fringe sides as the equal phase lines. A sequential tracking procedure similar to a technique used in [28] is

used to trace the fringe positions line by line from the top to the bottom of the picture to represent the fringe field as a polygon data structure.

To reduce the amount of data to store, a redundancy reduction algorithm [29] is activated whenever the temporary storage buffer of a certain polygon is filled. In this way the actual polygon is approximated by a subset of vertices of the original polygon within a certain given tolerance range.

If a fringe goes outside the field of view or a background object such as an airfoil resides inside the fringe field, the visible part of the fringe pattern can be handled by using the points on the boundary as edges of the fringes. Of course, the corresponding polygons may not be connected along the boundary of the background object because they may have different fringe orders. In order to establish the boundary test in a quick, easy and robust manner, it is not desirable to derive the boundary information from the fringe field itself. Therefore, the geometry of the test region (i.e. the coordinates of the boundary) is used to generate a binary valued mask which is compared pixel by pixel with the actual interferogram. The boundary of the test section may consist of a number of lines, and there may be several foreground areas or background areas imbedded in the field of view. The actual boundary may be generated from the known geometry of the set-up or may be manually entered and interactively drawn onto the screen.

Fig. 5 shows a typical example of the fringe coordinate extraction. An interferogram (Fig. 5a) is digitized over the whole field of view with low resolution. The white lines overlaying the display represent the extracted fringe sides, while the black line represents the border polygon which was input by hand before the coordinate extraction in order to mask off background objects and the part of the fringe field with high fringe density (in our implementation all the graphic is in color and therefore easier to distinguish from the displayed image).

The coordinates for each fringe polygon are stored in such an order that always the black part of the fringe is to the right of the polygon. This has some advantages when erroneous parts of the fringe field have to be corrected or fringe fields have to be combined. Lines may never be connected in a way that a "left" fringe side connects to a "right" one and vice versa and each line has to have a neighbor of different type.

The proposed segmentation with subsequent extraction of fringe sides has some advantages over tracking methods which follow the intensity minima or maxima along the fringes [23]. First it is more accurate because the fringe sides are better defined. In most practical cases the fringe pattern are sinusoidally modulated and the fringe sides are not affected as much by noise as are the fringe extrema due to the maximal slope at the sides. Another reason is that the method works well independently from the fringe density and the fringe contrast. Tracking methods tend to lose orientation in wide fringe areas and are unpredictable if the contrast is varying, because

they tend to run in the direction of maximal or minimal intensities. Also all points of the field of view have to be marked in order to avoid multiple tracking of the same fringe and to find all of the fringes. Because in the fringe side detection method two lines per fringe are read in one step, the accuracy is further increased over tracking methods. Another point is that the resulting line structures are of simpler type, because no line branchings occur. For this application tracking methods are much more unpredictable and slower, and too much intervening action would be necessary to use them successfully.

Enlarged subsections

As was discussed before, it may be necessary to digitize enlarged subsections to resolve regions with high fringe densities. The resulting fringe polygon field is then combined out of all the individual digitized and processed subsections, starting with the one with highest resolution. To handle the problem of partly overlapping polygon line fields, a boundary polygon is maintained for each subsection. This defines the definition area for each fringe polygon field. Upon combination of two overlapping fields, the border polygon of the one with higher resolution (priority) is used to intersect the lines of the other field. Both line fields are then connected at those intersection points. The new border polygon is the border of the combined areas.

Fig. 5b shows an enlarged digitized part of the interferogram as in Fig. 5a with the extracted fringe polygons overlaying. Fig. 5c shows a plot of the resulting polygon field which was combined from the lines in Fig. 5a and 5b and two other enlarged sections not shown.

3.4.2 Numbering, Error correction

If distortions are present in the interferogram, for instance, due to diffraction patterns, or there is insufficient contrast, or the fringe spacing exceeds the system resolution as in shock or boundary regions, disconnected fringes may occur and thus polygon segments representing fringes of different order may be connected. An example is given in Fig. 6, which is the extracted line field from Fig. 4f. In the lower middle portion of the interferogram there is a distortion of the fringe field due to a diffraction pattern, while in the lower right portion the lines are not resolved in the shock region.

In general, local information obtained from the close surrounding of these areas is insufficient to solve the problems, instead global knowledge about the entire fringe field is necessary. A complete correction of all the incorrectly linked polygon segments may be performed only during the fringe numbering. However, an error correcting scheme may be applied before starting the numbering

procedure. It uses the geometric parameters of the lines to detect suspicious lines. These are the shape features e.g. circularity (enclosed area divided by the perimeter squared), the distance of the polygon end points and the angles between polygon segments.

A fringe numbering scheme has to introduce the known numbering criteria into an algorithm. They are: (1) the fringe number difference of neighboring fringes must be zero or one, (2) fringes of different order do not intersect or touch each other, (3) fringes do not end inside the field of view unless they are circular fringes, and (4) the fringe number differences integrated along a closed line through the interferogram yield always zero. Furthermore the a priori known properties of the actual object have to be included. Different schemes have been developed to number various kinds of fringe fields [20,21].

One scheme suitable for the numbering of erroneously extracted line fields shall be described in some detail. The idea of the scheme is based on the fact that in general there are only a few locations which cover a small area, in which the fringe lines are falsely extracted, while the line field in most parts of the interferogram is represented correctly. The interferogram is divided into rectangular segments by a grid with suitably-sized meshes. The line segments inside the meshes are now numbered mesh by mesh, starting at the mesh with the maximal number of line segments and with a minimal number of inversion

points of fringe-counting (e.g. a mesh containing parallel lines). The algorithm now looks for the adjacent meshes in which the numbering can continue, i.e. which have at least two consecutive already numbered line segments at their common grid line. From these meshes, the one showing the best conditions is chosen. If the line numbering of the actual mesh is not in accordance with the numbering of the adjacent meshes, it is put back and handled later. In this way, the meshes containing disconnections are processed after all other meshes have been numbered. The numbering scheme now tries to number the line segments inside the erroneous meshes using the numbers already known in the neighboring meshes. If a line has to get different numbers, it is cut into two segments at the position where the angle between adjacent polygon segments is minimal. Another option is to cut at a position where a surface approximation onto the numbered polygon points exceeds a difference of more than a half order to a point of the actual line to be cut.

The procedure assigns relative fringe numbers. The absolute fringe order and direction of increase has to be specified at one location in the field to adjust the other numbers.

As an example of a relatively complex fringe pattern with respect to numbering, Fig. 7 shows the fringe lines of an interferogram of a membrane. The numbering grid is overlayed. The encircled numbers denote the order in which the meshes were processed by the algorithm. Note that the algorithm tends to number parts of the fringe field consisting of similar running lines in a monotonous manner. This is

the most basic rule used for fringe numbering, derived from the fact, that most physical object functions are monotonous and smooth in most areas of the field of view. If the fringe fields would not fulfil this basic requirement, a fringe numbering without further knowledge of the physical properties of the object would actually be impossible.

Fig. 8 shows the numbering grid used for numbering the line field in Fig. 6. The meshes containing the shock and the distorted area are detected by the algorithm because of their high number of inversion points. They are numbered after all other meshes have been processed. So the lines which could not be numbered uniquely will be cut somewhere in the mesh. The position where this is done, however, may not be the correct one. Often fringes of different order are connected through a shock without any indication of the existence of the shock (see e.g. Fig. 6). In this case, the area where the shock appears may be masked off by hand editing before starting the numbering (see Fig. 8).

In the edit mode, the fringe polygon fields may also be numbered manually by drawing a test line into the line field and numbering the intersected fringe lines by several commands using the cursor. Also all lines may be modified manually in the interactive edit mode before starting the numbering or the post processing.

3.4.3 Interpolation

After numbering the fringe lines, the OPD-function is defined at a set of contour lines, but most of the mathematical transformations to follow require interpolation of fractional fringe order numbers. Some methods for interpolation between random points on a surface have been discussed in [30] . An algorithm best suited in regard to computation time as well as numerical representation seems to be a local distance-weighted polynomial least squares approximation. At a given point (a,b) the coefficients of a two-dimensional polynomial of second order

$$P(x,y) = \sum_{k=0}^{2} \sum_{l=0}^{2-k} c_{kl} \, (x-a)^k \, (y-b)^l \qquad (4)$$

are estimated to minimize the quadratic form

$$Q = \sum_{r=1}^{N} (P(x_r,y_r) - z_r)^2 \, w((x_r-a)^2 + (y_r-b)^2) = \text{Min.} \qquad (5)$$

where $w(d^2)=\exp(-kd^2)$ is a weighting function, which gives more weight to the data points (x_r,y_r) having a shorter distance d to the point (a,b) than the more distant points. The additional advantage is that more distant points may be ignored in the computation. The solution of equation (5) is performed by solving a system of linear

equations (Gauss's method). The parameter k in the weighting function is chosen according to the local data point density. The whole fringe field may be represented with the polygon coefficients calculated on a regular grid. If a smooth approximation of the OPD-surface is desired a two-dimensional spline function may be defined at the meshes of a rectangular grid using only the zero and first order coefficients from the previously obtained polynomials.

An advantage of using a polynomial representation is the fact that an extrapolation of the fringe field is possible into regions blocked by background objects. As an example Fig. 9 shows an interpolated cross section through the numbered polygon field of Fig. 5c at z=c/3. Note, that the left side of the line is extrapolated over a region of the interferogram blocked off by the rotor system.

4. Reconstruction

A number of reconstruction algorithms such as Fourier transform methods, back-projection methods, and iterative methods are covered in the literature (see for instance [31]). Here a convolution backprojection algorithm with a filter function proposed in [32] was chosen, because it generally gives good results, is easy to implement, and is very efficient. The convoluted back-projection is given as

$$g_B(x,y) = \int_0^{\pi} \int_{-\infty}^{\infty} N_\phi(\xi) * F^{-1}\{|r|\}\, \delta(x\sin\phi + y\cos\phi - \xi)\, d\xi\, d\phi \qquad (6)$$

where $g_B(x,y)$ is the reconstructed field function in a horizontal plane (z=const), $N_\phi(\xi)$ are the cross sections through the fringe order function at angles ϕ to be convolved with the inverse Fourier transform of the abs-function. The integration of the convolved "projections" is done along the lines $L_\phi(\xi)$ which are expressed as

$$\delta(x\sin\phi + y\cos\phi - \xi) \qquad (7)$$

and over all the projections ϕ.

Fig. 10a shows a reconstruction of the flow field in a plane 8.28 percent chord above the blade obtained from the experimental data at 41 views for the angular interval from 8 to 40 and from 140 to 186 degrees in two degree intervals. The missing views are presumed to be zero (those interferograms have only a few or no fringes and were not evaluated). The resolution in the plane is 101 x 101 points, 101 rays were used in the projection data at each view (see Fig. 9). The time required for a reconstruction from 41 projections with 101 rays at a grid of 101 x 101 points is approximately 24 sec. CPU time on a VAX 11/780.

The reconstruction gives a map of the refractive index in the plane. Because the refractive index of gases is proportional to the density ρ (Gladstone-Dale relation)

$$\rho/\rho_o = (n - 1) / (n_o - 1) \qquad (8)$$

the density may directly be calculated. Other flow properties as pressure may be obtained by assuming isentropic flow. The perturbation velocity is derived by application of a form of the energy equation to the blade fixed flow problem.

The lines in Fig. 10a are contour lines of the perturbation velocity. This result may be compared to a cross section through a numerically obtained solution [33] which is shown in Fig. 10b. The basic features of the flow field, the shock position, and the amplitudes are very well confirmed. A slight difference appears in the velocity profiles across the chord in the tip region of the blade which can possibly be attributed to a lambda-shock, which can not be predicted by the nonviscous, potential numerical code.

A more detailed discussion of the reconstruction results and a comparison with hot wire and pressure measurements is given in [34].

5. Conclusions

The features of an image processor based system for interferogram analysis have been described. The system contains algorithms for all steps of digital interferogram processing from image processing techniques such as digitization, enhancement, segmentation to graphic data processing techniques such as fringe coordinate extraction, merging of line fields, error correction, fringe numbering, and approximation techniques for interpolation of 2-D fringe fields. All the modules may be called interactively and editing features are available to process interferograms even if they are of poor quality. The interactive modes are fully supported by graphic visualization. An application to the reconstruction of a 3-D flow field, which was recorded by holographic interferometry at several views around the field, was given. It showed that the evaluation of the interferograms could be considerably improved and accelerated by the digital techniques compared to manual evaluation. The full analysis of the flow field under investigation would hardly have been possible if the data had to be analysed manually.

However, in the described implementation some information has to be input manually even for interferograms of good quality. These are the geometric reference points, the decision whether blown up subsections should be digitized, choosing of an optimal enlargement factor, entering of background border polygons, and a reference number for the

fringe numbering. In order to use this system in a standard test facility the interactive action can be further reduced by using the same information for series of interferograms taken under similar conditions.

6. Acknowledgments

During this work one of the authors (F.B.) was holding an NRC Resident Research Associateship at the NASA-Ames Research Center. Part of the interferogram evaluation software was developed previously by one of the authors (F.B.) at the Max-Planck-Institut für Strömungsforschung in Göttingen, West Germany. The authors wish to acknowledge the efforts of Mr. John Kittleson at the Aeromechanics Laboratory for providing the quality interferograms used in the tomographic reconstruction process. The enthusiastic support and contribution of Dr. Sanford S. Davis and George Lee at NASA Ames Research Center are gratefully acknowledged. The inspiration and unselfish support of Dr. Fredric H. Schmitz at Aeromechanics Laboratory made this project possible.

7. References

1. Trolinger, J. D., AGARDograph 186, 1974

2. D. A. Johnson, and W. D. Bachalo, AIAA Paper 78-1117, July 1978

3. J. K. Kittleson, Ninth European Rotorcraft Forum, Paper No. 8, Sept. 13-15, 1983, Stresa, Italy

4. G. Lee, NASA Technical Memorandum 84325, Jan. 1984

5. R. Snyder and L. Hesselink, Appl. Opt. 23(20), 3650 (1984)

6. J. H. Bruning, D.R. Herriott, J.E. Gallagher, D.P. Rosenfeld, A.D. White, and D.J. Brangaccio, Appl. Opt. 13(11), 2693 (1974)

7. W. R. Fischer, H.-A. Crostack, and H.-D. Steffens, Laser 79 Opto-Electronics, Munich 2/6 July 1979, Conf. Proc., IPC Science and Technology Press, London 1979, pp. 404-411

8. T. Yatagai, and T. Kanou, Opt. Eng. 23(4), 357 (1984)

9. R. Smythe, and R. Moore, Opt. Eng. 23(4), 361 (1984)

10. ZYGO Automatic pattern processor, Technical description, Zygo Corp., (1981)

11. Dändliker, R., in "Progress in Optics", Vol. 17, Chap. 1
E. Wolf, Ed., North-Holland, Amsterdam (1980)

12. M. Takeda, H. Ina, and S. Kobayashi, J. Opt. Soc. Am. 72, 156
(1982)

13. K. H. Womack, Opt. Eng. 23(4), 391 (1984)

14. M. Schlüter, Optics and Laser Technology 12, 93 (1980)

15. D. W. Robinson, Appl. Opt. 22(14), 2169 (1983)

16. D. A. Tichenor, and V.P. Madsen, Opt. Eng. 18(5), 469 (1979)

17. S. Nakadate, N. Magome, T. Honda, and J. Tsujiuchi,
Opt. Eng. 20(2), 246 (1981)

18. S. Nakadate, T. Yatagai, and H. Saito, Appl. Opt. 22(2), 237 (1983)

19. T. Yatagai, S. Inabu, H. Nakano, and M. Suzuki,
Opt. Eng. 23(4), 401 (1984)

20. F. Becker, "Zur automatischen Auswertung von Interferogrammen",
Mitteilungen des Max-Planck-Institutes, Göttingen, Nr. 74, (1982)

21. F. Becker, G. E. A. Meier, and H. Wegner, in "Applications of Digital Image Processing IV", Andrew G. Tescher, ed., Proc. SPIE 359, 386 (1982)

22. H. S. Cline, A. S. Holik, W. E. Lorensen, Appl. Opt. 21(24), 4481 (1982)

23. W. R. J. Funnel, Appl. Opt. 20(18), 3245 (1981)

24. A. Rosenfeld, and A. Kak, "Digital Picture Processing", Academic Press, New York (1976)

25. To Russel Hsing, Opt. Eng. 23(3), 288 (1984)

26. J. J. Snyder, Appl. Opt. 19, 1223, (1980)

27. J. B. Schemm, and C. M. Vest, Appl. Opt. 22(18), 2850 (1983)

28. A. K. Agrawala, and A.V. Kulkarni, Computer Graphics and Image Processing 6, 538 (1977)

29. U. Ramer, Computer Graphics and Image Processing 1, 244 (1972)

30. D. H. McLain, Computer Journal 17(4), 318 (1974)

31. G. T. Herman, (ed.), "Image Reconstruction from Projections, Implementation and Applications", Topics in Appl. Phys. 32, Springer, Berlin (1979)

32. L. A. Shepp, and B. F. Logan, IEEE Trans. NS-21(3), 21 (1974)

33. F. X. Caradonna, "The Transonic Flow on a Helicopter Rotor", Ph.D. Dissertation, Stanford Univ., Stanford, Calif., (3,1978)

34. J. K. Kittleson, and Y. H. Yu, AIAA Paper No. 85-0370, Jan. (1985)

Table 1. Execution times of some Hardware- and Software-modules

Function	approx. CPU time
Digitization, Look-Up-Table operations	1/30 sec
Averaging over N frames	N/30 sec
Convolutions† (k=kernel elements)	K/30 sec
Binary operations (smoothing, shrinking, expanding)	K/30 sec
Subtraction of approximated background	16 sec
Application of floating threshold method	14 sec
Extraction of fringe coordinates*	30 sec
Merging of line fields*	10 sec
Numbering, error correction*	10 sec
Interpolation* (comp. of coefficients per polynom)	0.05 sec

†) For image processor equipped with three memory pages

*) Times depend on the complexity of the image and the number of fringes. The times given are for a typical example like Fig. 5

Figures

Fig. 1 Top view of the holographic set-up with sample interferograms taken at different angles

Fig. 2 Sketch of the image processing hardware

Fig. 3 Example of one-dimenional processing

3a Floating threshold fringe segmentation

3b Demonstration of the threshold fringe segmentation on a scan line of an actual interferogram

3c Digitized interferogram (182.5) with segmented cross-sections superimposed

3d Evaluation of an enlarged section of the same interferogram as in Fig. 3c

3e Fringe order function along cross section 3 of interferogram 182.5 after combination of several enlarged subsections and rational spline interpolation

Fig. 4 Example of fringe segmentaion, binarization

4a Enlarged digitized subsection of interferogram (184.5) with superimposed grid of meshes of size 64 x 64

4b Floating threshold method applied to lines of Fig. 4a

4c Floating threshold method applied to columns of Fig. 4a

4d Thresholding after background subtraction, computed on the grid in Fig. 4a

4e Combination of methods b,c, and d

4f Result after binary smoothing and shrinking - expanding operations applied to Fig. 4e

Fig. 5 Example of fringe polygon extraction and merging of enlarged digitized subsections

5a Original digitized interferogram (8.5), extracted fringe polygons are overlayed in white, the border polygon is written in black

5b Enlarged digitized part of the same interferogram, extracted fringe polygons are overlayed

5c Plot of the resulting polygon field merged from 6a and 6b and two other enlarged sections not shown

Fig. 6 Extracted line field of Fig. 4t, showing disconnected lines in an area disturbed by a diffraction pattern and in a shock region

Fig. 7 Fringe numbering
Example of a complex fringe pattern with several minima and maxima, encircled numbers give the order in which the meshes were processed

Fig. 8 Numbered and error corrected line field of Fig. 5c with numbering grid

Fig. 9 Interpolated fringe order function along a cross-section at z=c/3 through the numbered line field of Fig. 5c, showing extrapolation to the left. The symbols mark the coordinates of the fringe polygons in the cross-section

Fig. 10 Reconstruction of the flow field in a horizontal plane at z/c=0.0828 above the blade
The blade rotates clockwise, leading edge is at x/c=0.
(c is the chord length of the blade, Ro is the blade radius)

10a Perturbation velocity contours in ft/s as reconstructed from cross-sections through 41 interferograms, at 101 x 101 points

10b Perturbation velocity contours at the same height above the blade as given by a numerical solution of the flow problem

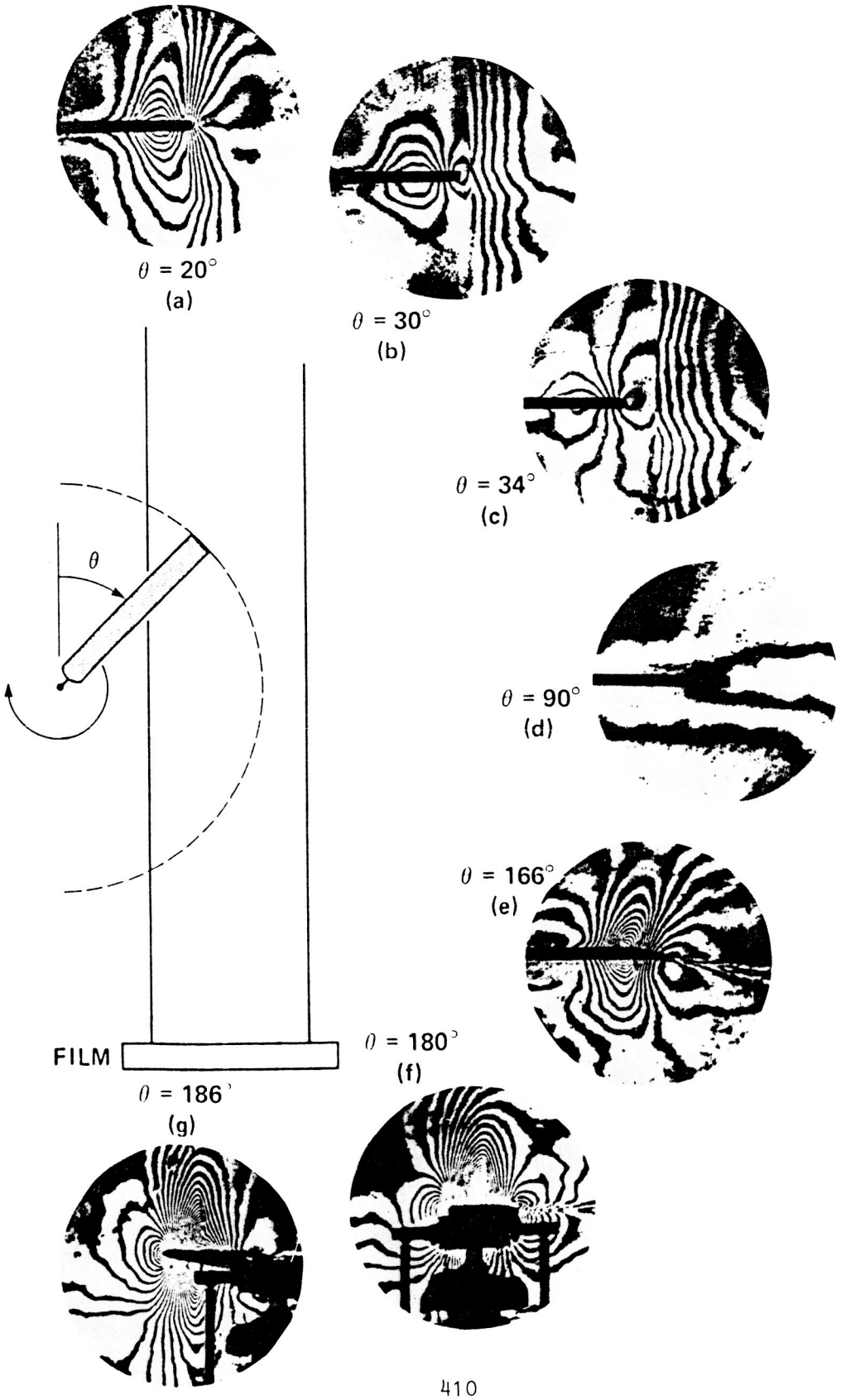
θ = 20°
(a)
θ = 30°
(b)
θ = 34°
(c)
θ
θ = 90°
(d)
θ = 166°
(e)
θ = 180°
(f)
FILM
θ = 186°
(g)

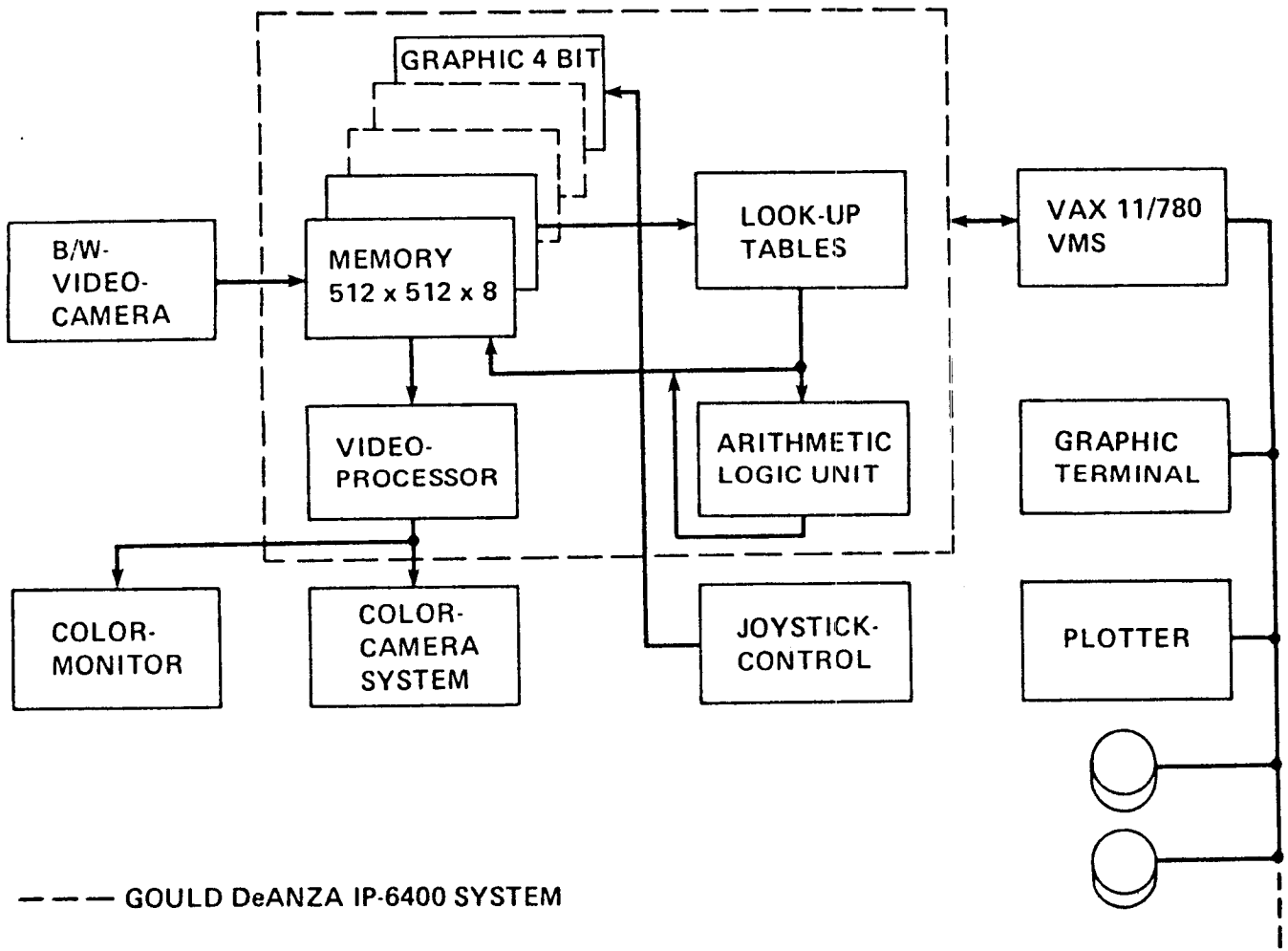
GRAPHIC 4 BIT
B/W-
VIDEO-
CAMERA
MEMORY
512 x 512 x 8
LOOK-UP
TABLES
VAX 11/780
VMS
VIDEO-
PROCESSOR
ARITHMETIC
LOGIC UNIT
GRAPHIC
TERMINAL
COLOR-
MONITOR
COLOR-
CAMERA
SYSTEM
JOYSTICK-
CONTROL
PLOTTER
— — — GOULD DeANZA IP-6400 SYSTEM

Fig 3a top

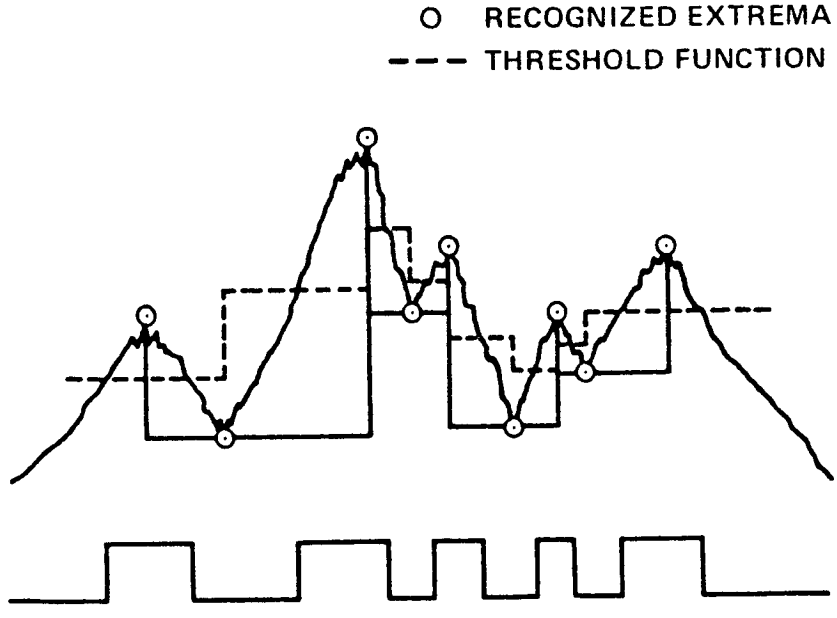

Fig 3b top

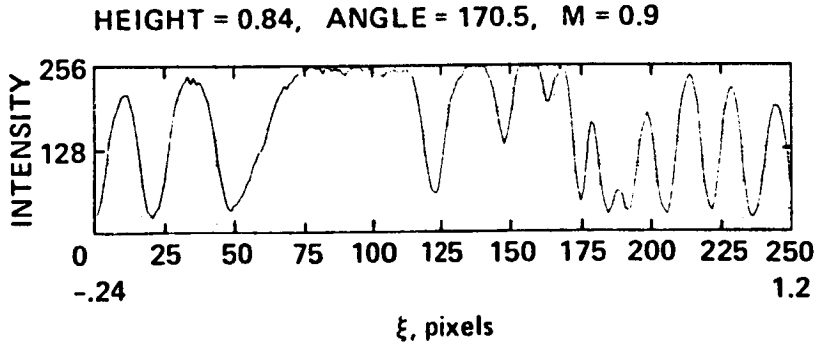
HEIGHT = 0.84, ANGLE = 170.5, M = 0.9
INTENSITY
256
128
0
25
50
75
100
125
150
175
200
225
250
-.24
1.2
ξ, pixels

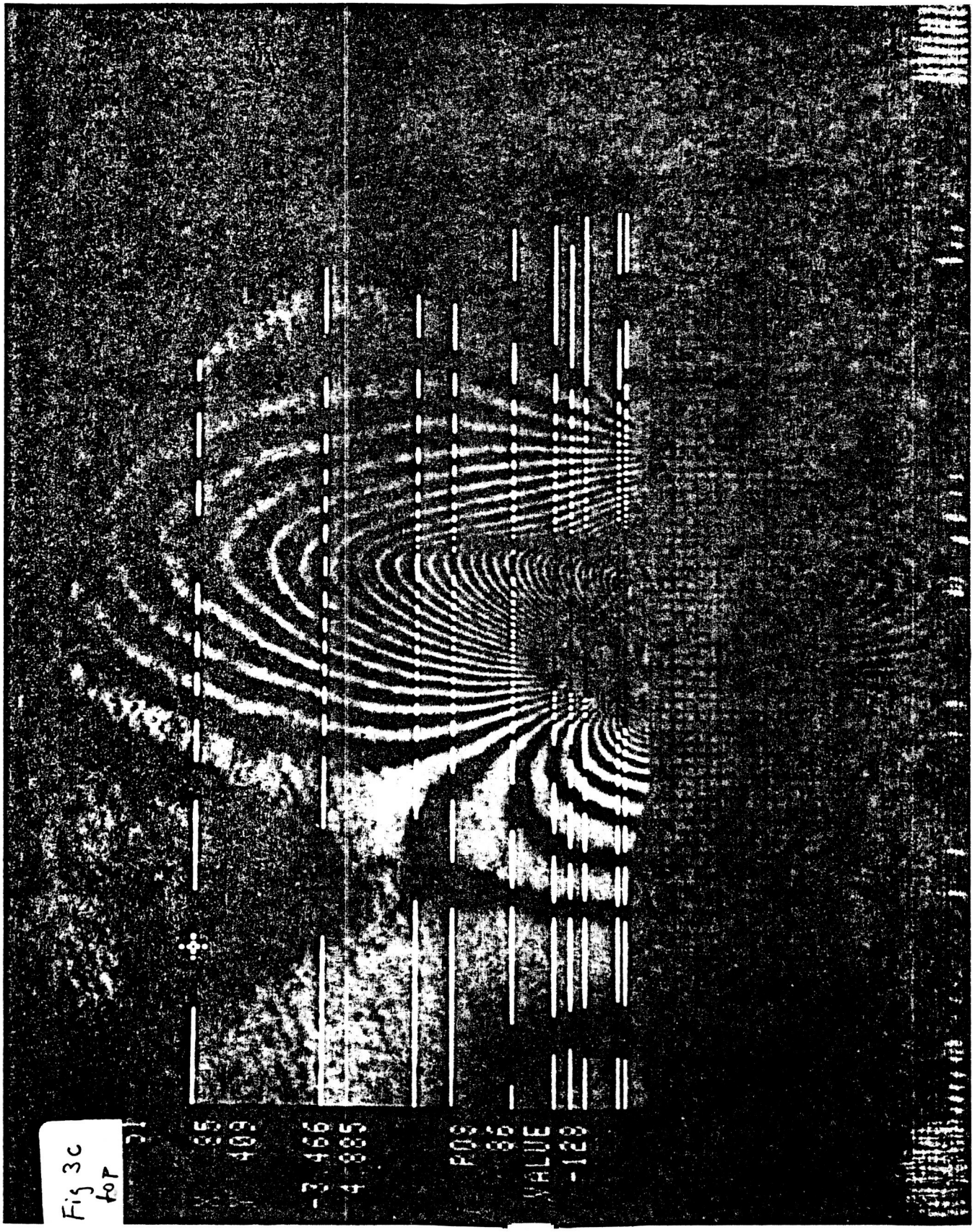

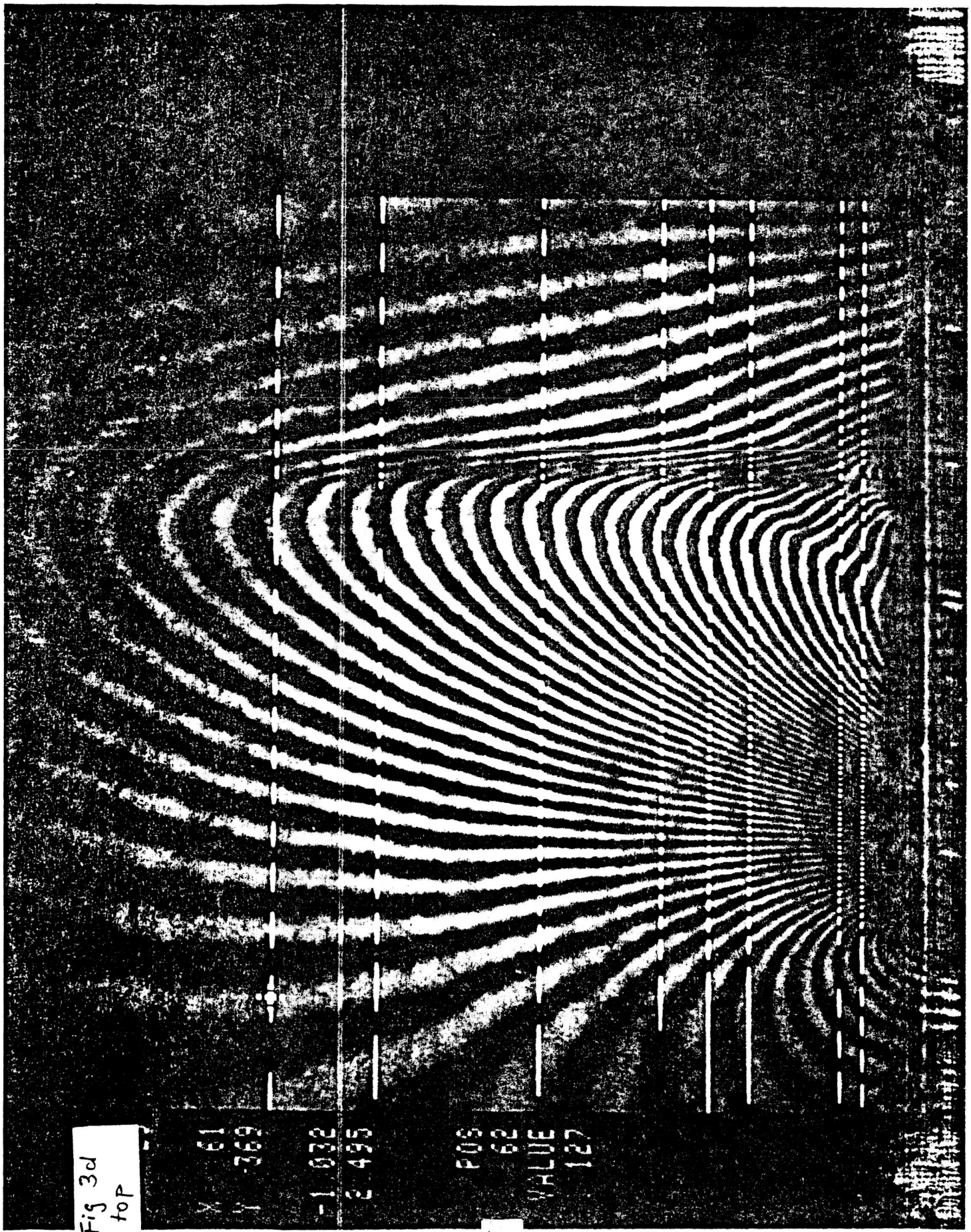

Fig 3d
top

Fig 3e top

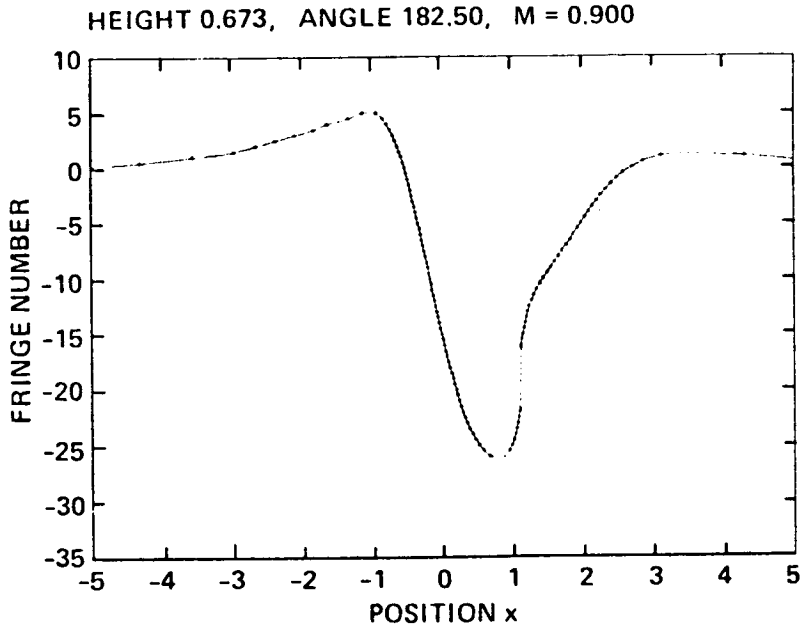
HEIGHT 0.673, ANGLE 182.50, M = 0.900
FRINGE NUMBER
10
5
0
-5
-10
-15
-20
-25
-30
-35
-5
-4
-3
-2
-1
0
1
2
3
4
5
POSITION x

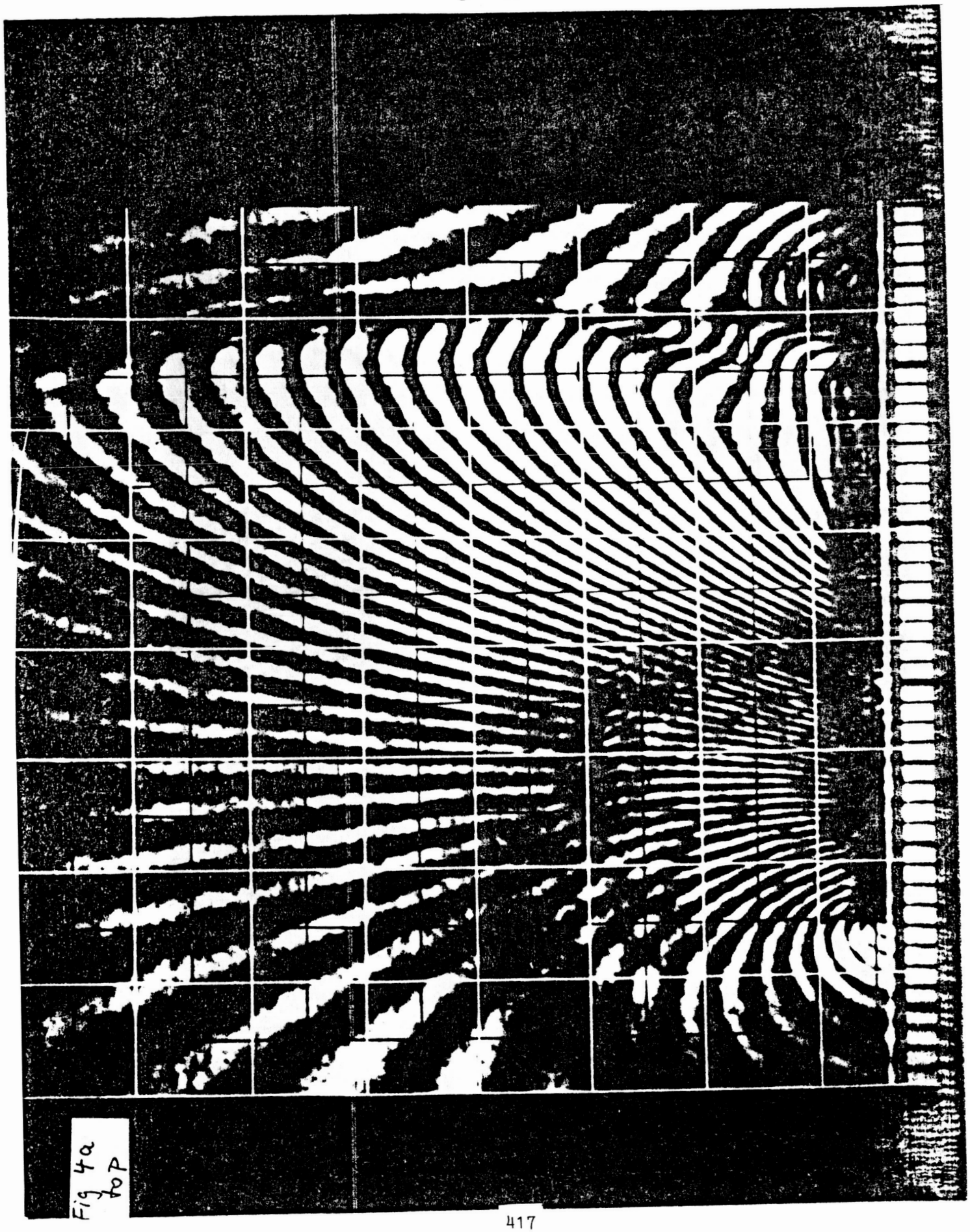

Fig 4a
top P

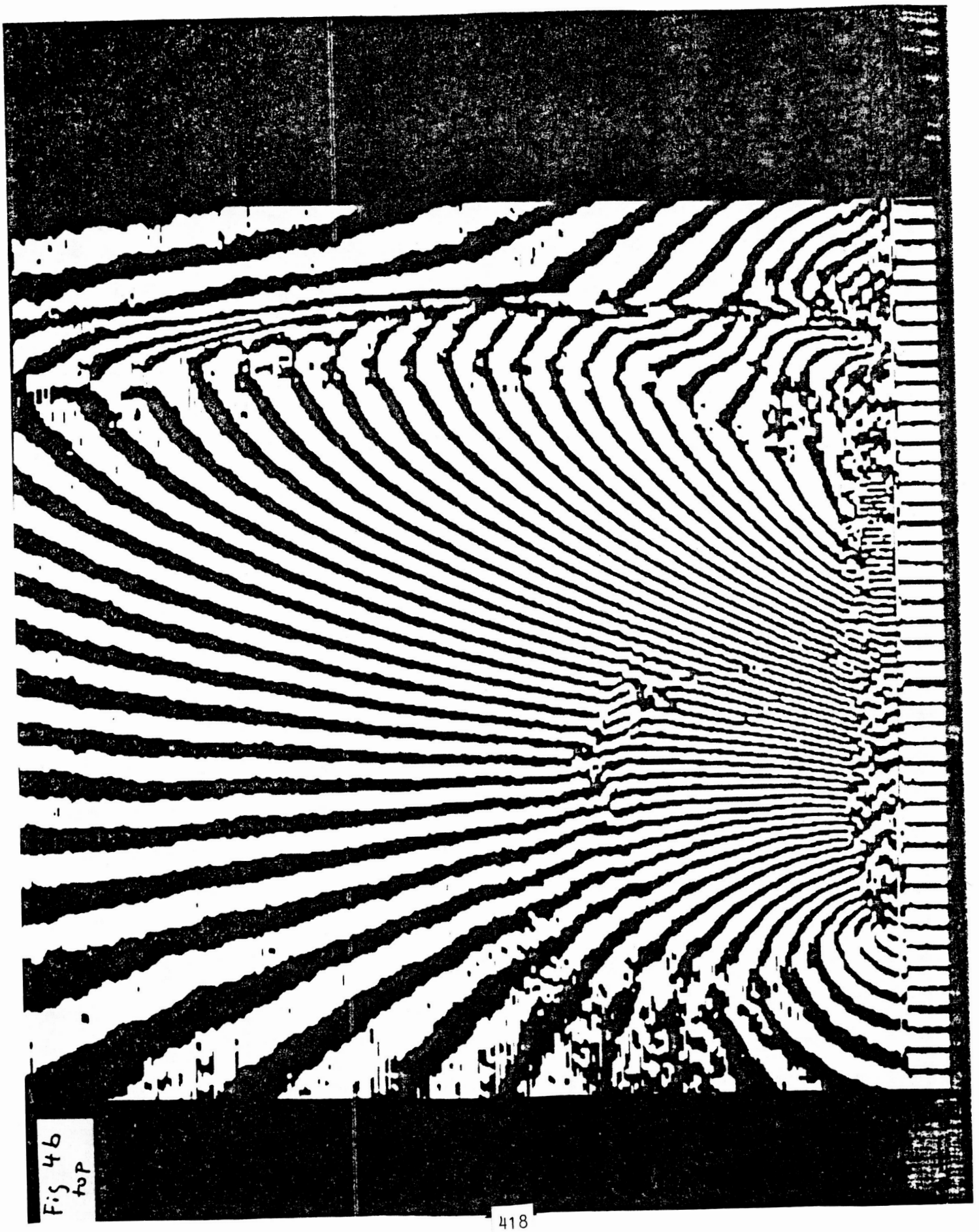

Fig 46
top

Fig 4c
top

Fig 4d
top

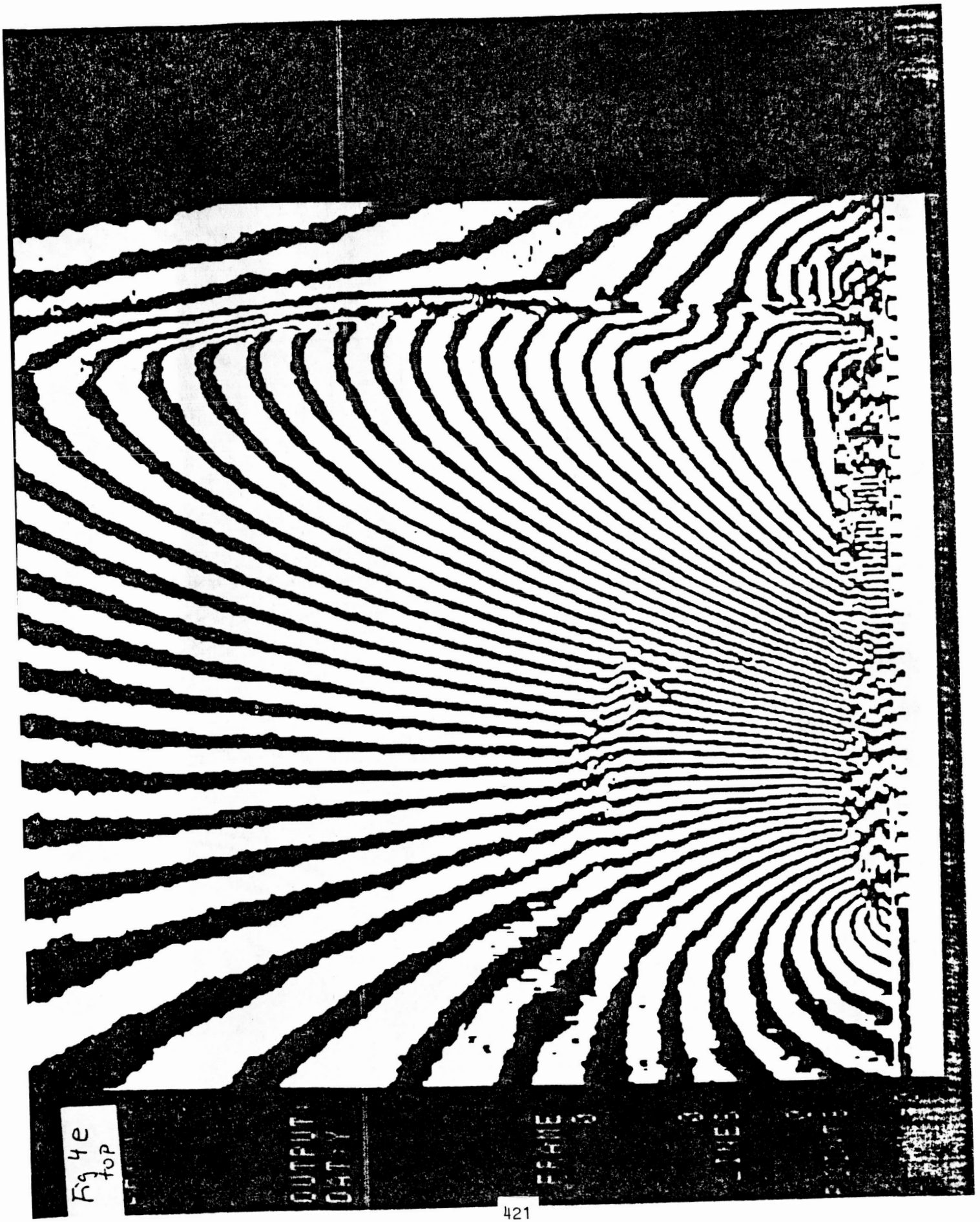

Fig 4e top

Fig 4 f
for P

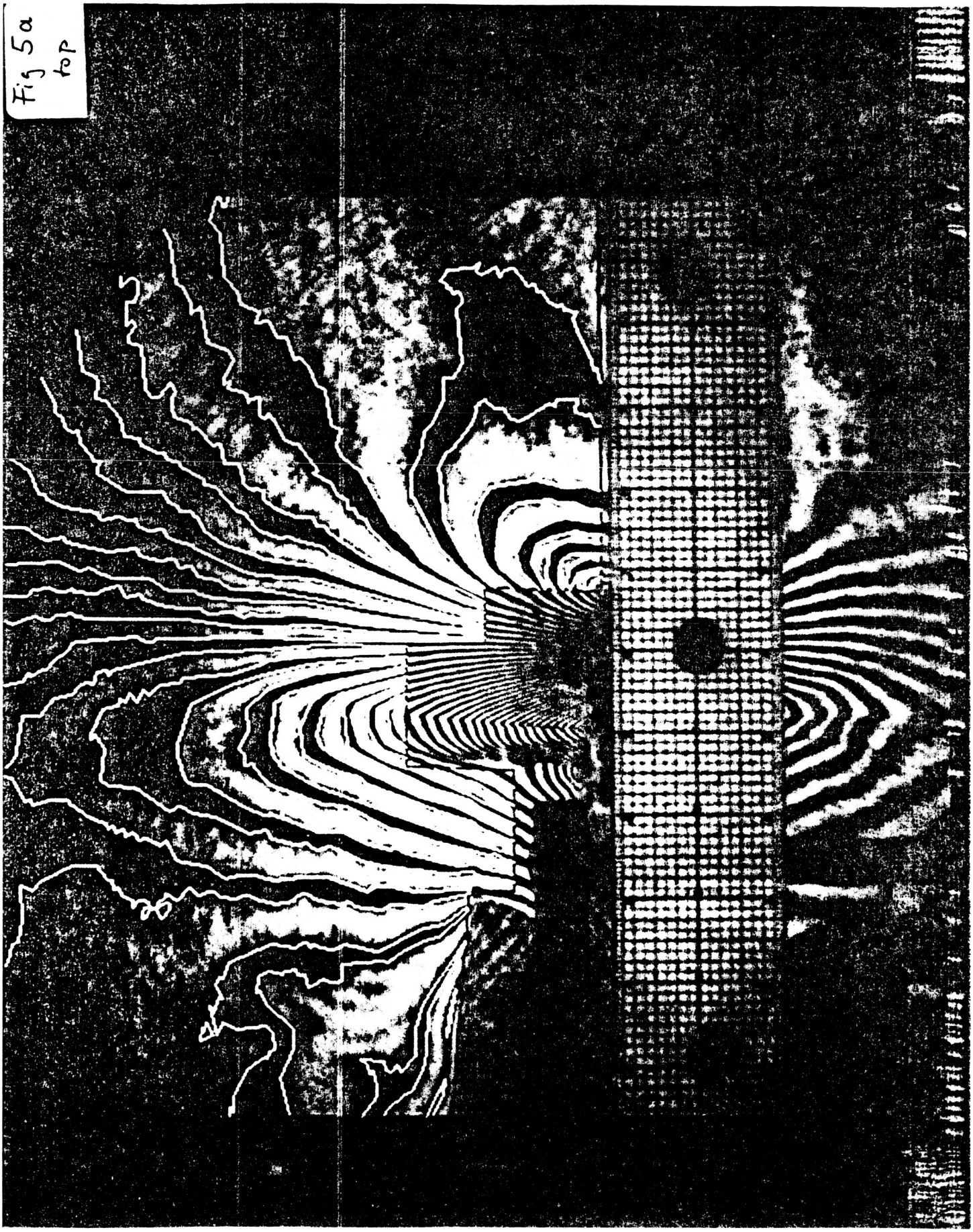

Fig 5b
top

Fig 5c

top

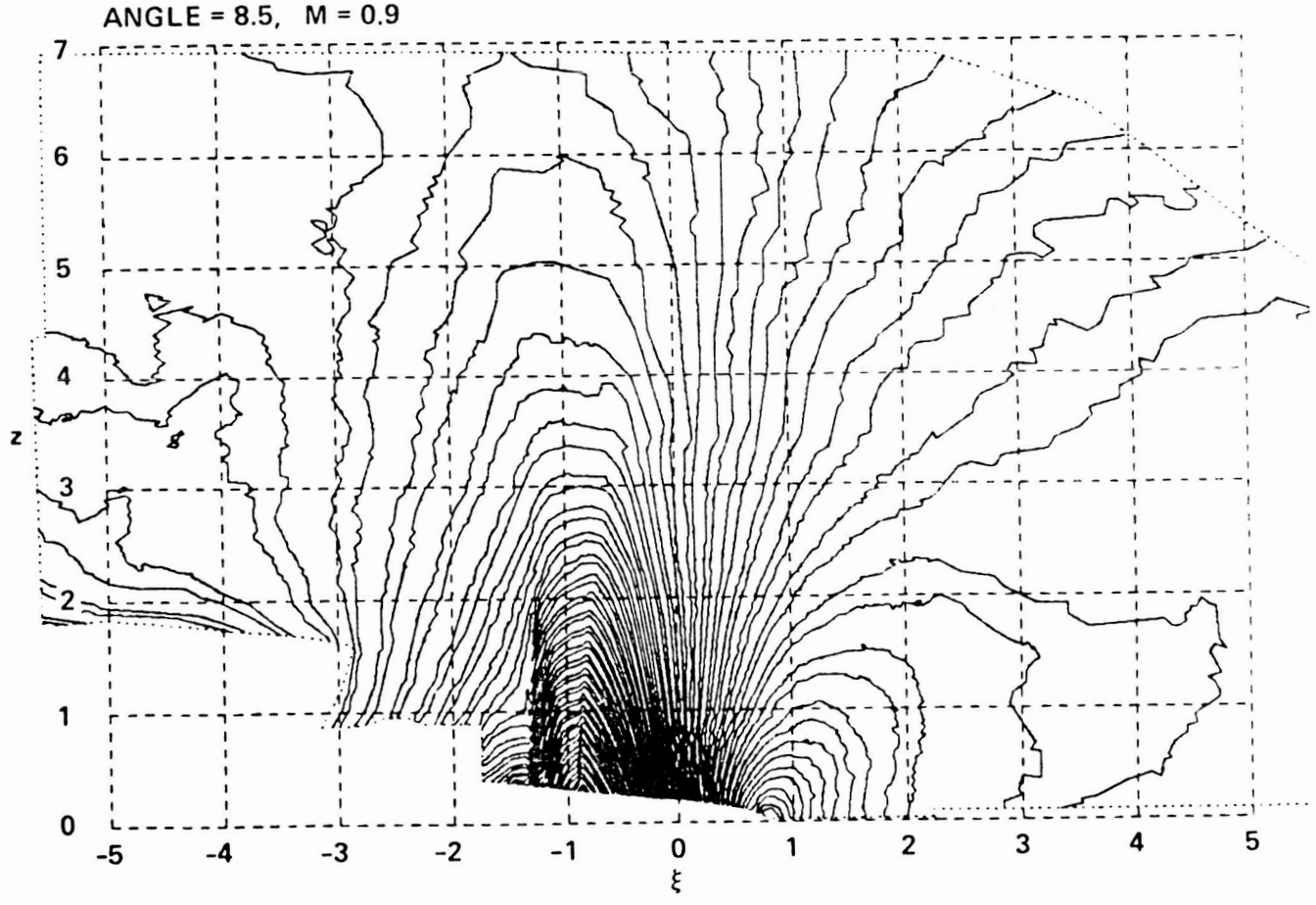

Fig 6 top

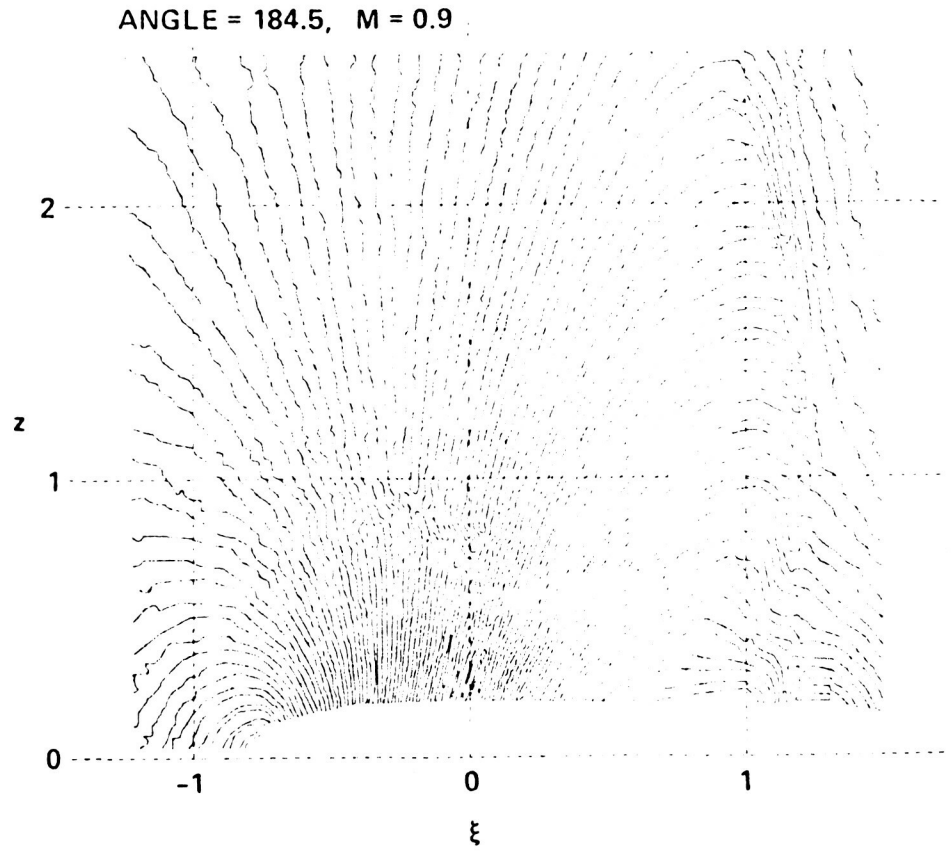

ORIGINAL PAGE IS
OF POOR QUALITY

Fig 7 top

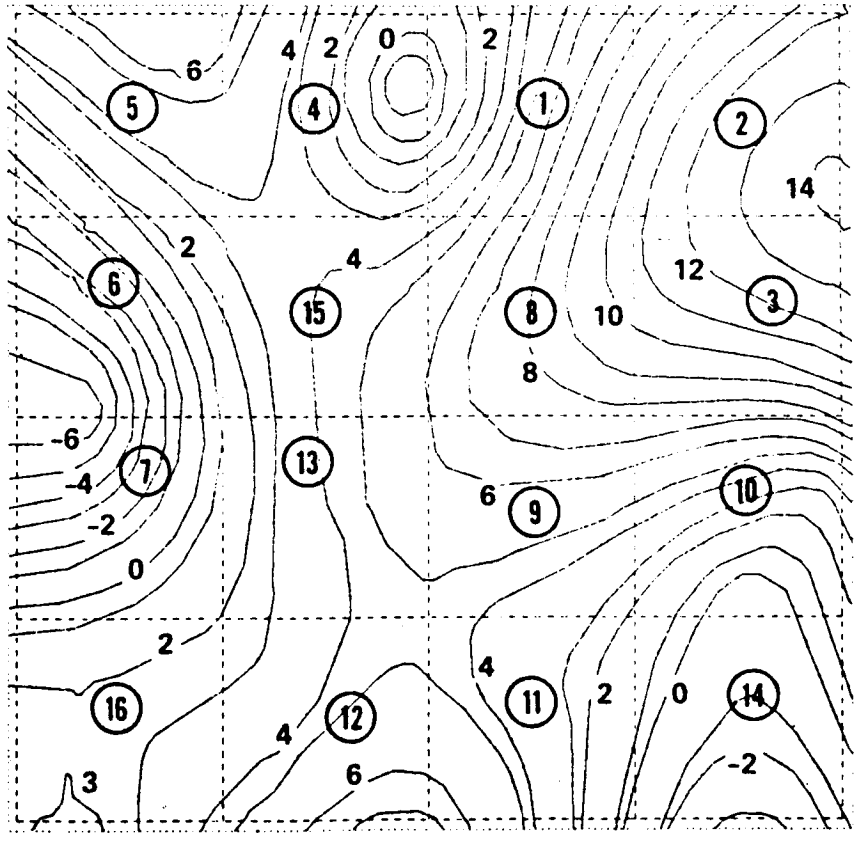
6
4
2
0
2
5
4
1
2
14
2
4
12
6
15
8
10
3
8
-6
7
13
6
9
10
-4
-2
0
2
4
16
12
11
2
0
14
4
-2
3
6

Fig 8 top

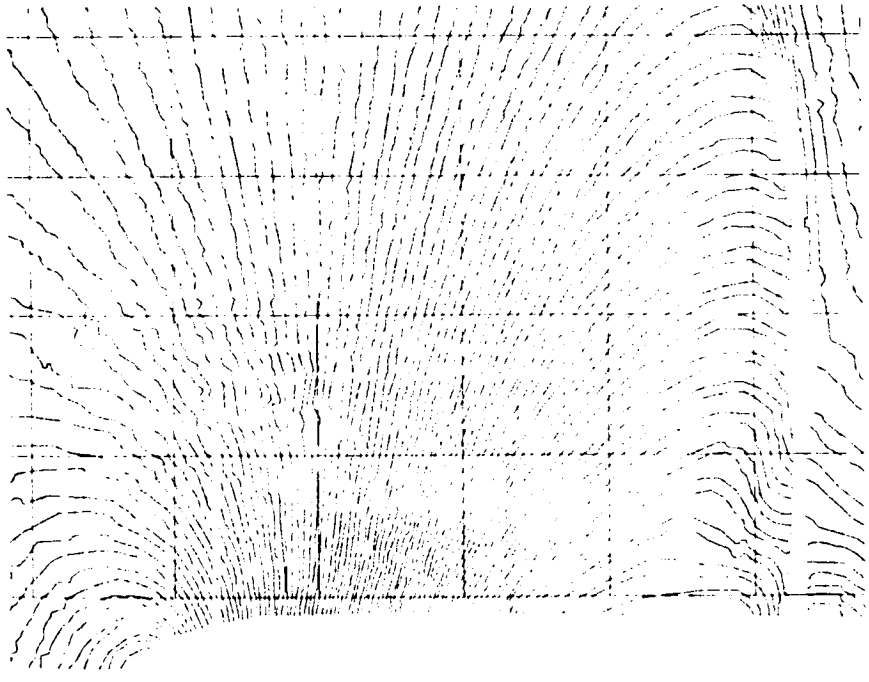

Fig 9 top

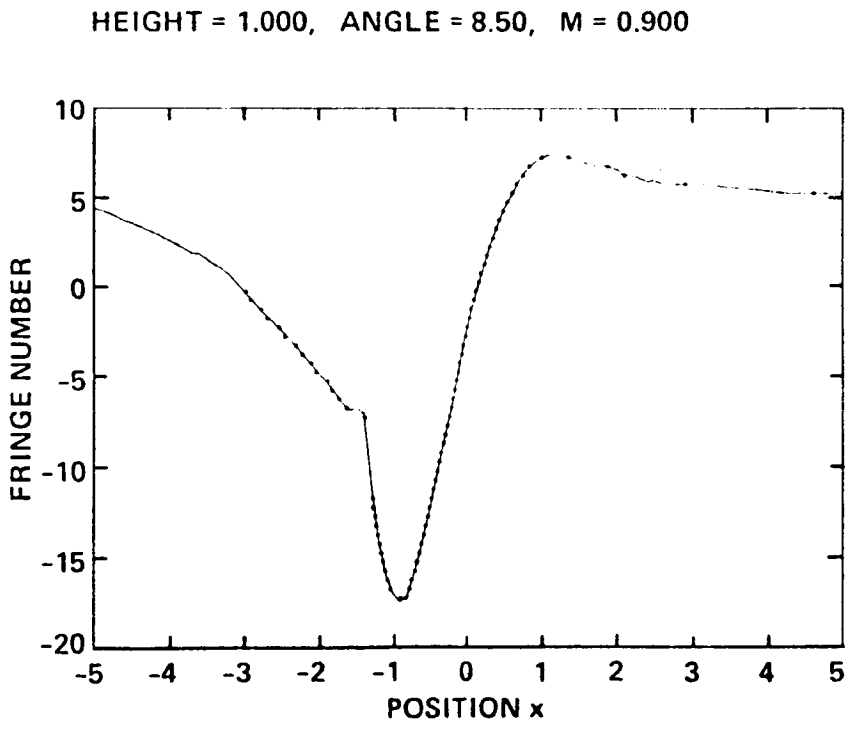
HEIGHT = 1.000, ANGLE = 8.50, M = 0.900
FRINGE NUMBER
10
5
0
-5
-10
-15
-20
-5
-4
-3
-2
-1
0
1
2
3
4
5
POSITION x

Fig 10 a top

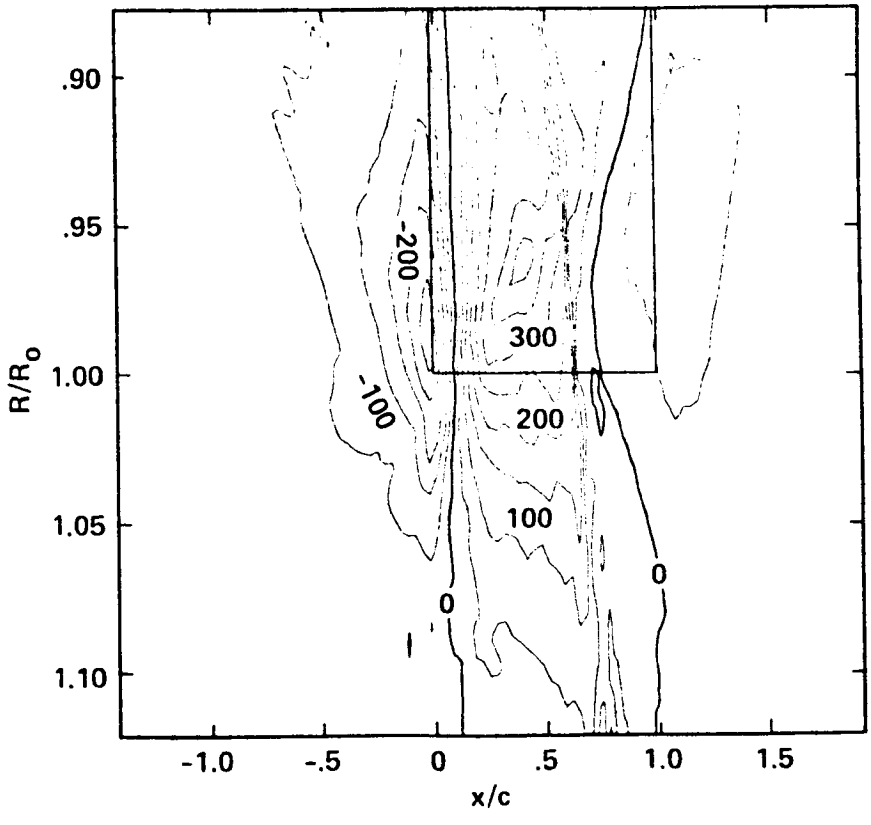

Fig 10 b top